Naval Research Laboratory
Washington, DC 20375-5320

NRL/6170/MR—2022/2

In-Situ Investigation of Ambient and Sub-Ambient Sodium-Sulfur Discharge Mechanism in Glyme Ethers

RACHEL CARTER

Surface Chemistry Branch
Chemistry Division

March 29, 2021

REPORT DOCUMENTATION PAGE

Form Approved
OMB No. 0704-0188

1. REPORT DATE *(DD-MM-YYYY)*	**2. REPORT TYPE**	**3. DATES COVERED** *(From - To)*
29-03-2022	NRL Memorandum Report	04/08/2019 – 04/08/2020

4. TITLE AND SUBTITLE

In-Situ Investigation of Ambient and Sub-Ambient Sodium-Sulfur Discharge Mechanism in Glyme Ethers

5a. CONTRACT NUMBER

5b. GRANT NUMBER

5c. PROGRAM ELEMENT NUMBER
NISE

6. AUTHOR(S)

Rachel Carter

5d. PROJECT NUMBER

5e. TASK NUMBER

5f. WORK UNIT NUMBER
N2U5

7. PERFORMING ORGANIZATION NAME(S) AND ADDRESS(ES)

Naval Research Laboratory
4555 Overlook Avenue, SW
Washington, DC 20375-5320

8. PERFORMING ORGANIZATION REPORT NUMBER

NRL/6170/MR--2022/2

9. SPONSORING / MONITORING AGENCY NAME(S) AND ADDRESS(ES)

Naval Research Laboratory
4555 Overlook Avenue, SW
Washington, DC 20375-5320

10. SPONSOR / MONITOR'S ACRONYM(S)
NRL/NISE

11. SPONSOR / MONITOR'S REPORT NUMBER(S)

12. DISTRIBUTION / AVAILABILITY STATEMENT

DISTRIBUTION STATEMENT A: Approved for public release; distribution is unlimited.

13. SUPPLEMENTARY NOTES
Karle Fellowship

14. ABSTRACT

This work identifies optimal chemical (monoglyme) and environmental environments (0°C) for the reaction between sodium and sulfur, so that this high energy pairing may be exploited for low-cost energy storage ($1/kWh). It is of particular interest to naval applications that sub-ambient temperatures (here 0°C) enhance the system performance, since air and sea operations often require this temperature range.

15. SUBJECT TERMS

16. SECURITY CLASSIFICATION OF:			**17. LIMITATION OF ABSTRACT**	**18. NUMBER OF PAGES**	**19a. NAME OF RESPONSIBLE PERSON**
					Rachel Carter
a. REPORT	**b. ABSTRACT**	**c. THIS PAGE**	U	25	**19b. TELEPHONE NUMBER** *(include area code)*
U	U	U			(202) 404-6291

Standard Form 298 (Rev. 8-98)
Prescribed by ANSI Std. Z39.18

This page intentionally left blank.

CONTENTS

FIGURES

Figure 8- Full UV-vis spectra from Figure 7A collected ~every 2 minutes. Each spectra is color coded with approximate visual color of the electrolyte solution.

Figure 9- Electrochemical and optical analyses of discharge in G1 (left column), G2 (center column), and G4 (right column). **A, E, I** Voltage during C/2 galvanostatic discharge, **B, F, J** RGB pixel analysis including pixel ratio and image brightness aligned with discharge voltage, and **C, G, K** the resulting average electrolyte color bar. Distinct changes in electrolyte color are indicated with grey vertical lines and notated with the polyanion responsible for these changes. **D, H, L** Photographs of the optical cell window at completion of the electrochemical discharge.

Figure 10- **A** Voltage during C/2 galvanostatic discharge and subsequent charge in 1M $NaPF_6$ G2 electrolyte (left y) and RGB pixel ratio (right y). **B** Photographs of optical cell revealing electrolyte color change at key voltage points during the discharge and subsequent charge. Arrows indicate approximate color. **C** and **D** Replicates of **A**.

Figure 11- A Voltage during C/2 galvanostatic discharge in G2 at 20°C (grey) and 0°C (blue). **B** the electrolyte filled gap between the sulfur cathode (left) and sodium anode (right). Two cases are shown at each temperature: the initial case, and at the completion of a discharge in **A**.

TABLES

Table 1- Material properties of glyme ether solvents at 20°C relevant to solubility and electrochemical performance.[1]

This page intentionally left blank.

EXECUTIVE SUMMARY

Herein the results of a 1 year Karles fellowship beginning in August of 2019 is presented. This work identifies optimal chemical (monoglyme) and environmental environments (0°C) for the reaction between sodium and sulfur, so that this high energy pairing may be exploited for low-cost energy storage ($1/kWh). It is of particular interest to naval applications that sub-ambient temperatures (here 0°C) enhance the system performance, since air and sea operations often require this temperature range.

We characterize the reaction between sodium and sulfur in ambient conditions.. Intermediate discharge products manifest with distinct colors allowing us to use novel *in situ* optical investigation to chart the reaction products with cell voltage and capacity. Image analysis of the electrolyte between the sulfur working electrode and sodium counter electrode allow for the red, green and blue (RGB) image pixilation and image brightness to be assessed. Optical analysis facilitates detection and characterization of intermediate products across a broader concentration range that is not accessable by more complex *in situ* UV-Vis spectroscopy. We use *in situ* optical microscopy to compare the ambient discharge mechanism in electrolytes from the glyme family ranging from monoglyme (G1) to tetraglyme (G4), which are known for sodium stabilty. G1 provides the best sodium storage capacity and most reversible reaction pathway, while G4 provides the worst. G2 (diglyme) falls between them. Low temperature operation (0°C) of G2 identifies unexpected improved storage capacity and reaction path. These findings will aid in design of an effective ambient sodium sulfur electrolyte environment.

This page intentionally left blank.

IN SITU INVESTIGATION OF AMBIENT AND SUB-AMBIENT SODIUM-SULFUR DISCHARGE MECHANISM IN GLYME ETHERS

1. OBJECTIVE

1.1 Topline Objectives

The energy dense battery chemistry, sodium-sulfur, is not realized under ambient temperatures due to lack of understanding of the discharge mechanism. This program utilized NRL's unique *in situ* optical cell to investigate the reaction behavior to promote its utility in the US Navy. We elucidate unstable, intermediate discharge products in sodium sulfur cells and correlate to distinct battery voltages in order to enable a rechargeable (and cycleable) system. With this novel *in situ* method, electrolyte solvents and operating conditions are modulated to find a system capable of supporting room temperature conversion of sulfur to high-energy sodium sulfide product for electrochemical charge storage.

1.2 Motivation

In the 1960s, the Ford Motor Company first proposed a sodium-sulfur battery for vehicle electrification.[2] The electrode pair is highly desirable due to the global abundance of both materials[3] and the high theoretical energy density of the reaction (~1400 Wh/kg).[4-5] However, the poorly understood, multistep conversion of the reactants to the Na_2S discharge product has prevented its realization to date.[6-10] A portion of the reaction can be harnessed by liquefying the reactants at high temperatures (>300°C) to simplify the conversion and enable cyclability.[2] This strategy is commercially available; however, the safety and cost of operating at high temperature prevents widespread use.[11]

In order to facilitate ambient operation we need to chart the ideal discharge mechanism, and understand how features like electrolyte composition, charge rate and electrode properties influence this behavior. This effort particularly focuses on the role of the electrolyte solvent. We investigate discharge behavior in three different glyme based ether electrolytes via optical microscopy and also interrogate the influence of these solvents on the anode and cathode battery electrodes. All the glyme ethers have demonstrated stable sodium plating but their chain lengths, growing from G1 (monoglyme) to G4 (tetraglyme), facilitate differing material properties like phase change temperatures, viscosities, and polysulfide solubility (Table S1).[12] Therefore, it is important to understand how solvent properties influence the sodium-sulfur discharge mechanism so that an optimal electrolyte solvent or solvent cocktail can be identified.

1.3 Technical Approach

Herein, the electrochemical reaction between sodium and sulfur is investigated in three glyme electrolytes using an *in situ* electrochemical optical cell. A unique, air-tight, electrochemical-optical cell is utilized to characterize, *in situ*, the electrolyte for sodium sulfur cells while electrical current is applied or drawn, replicating battery charge and discharge behavior. Fig 1 shows that during the discharge, elemental sulfur, assembled in S_8 rings, is reacted with sodium to form Na_2S. This process can involve up to 8 intermediate products

Manuscript approved March 14, 2022

including: Na_2S_n, $1<n\leq 8$. The electrochemical and chemical instability of these compounds facilitate their dissolution into the electrolyte, a behavior difficult to reverse, but easily observed through dramatic color changes (crimson, teal and yellow) and strong vibrational stretch modes. Therefore, if intermediate products solubilize in the electrolyte, they can be identified and quantified with respect to the cell's electrochemical potential during charge and discharge to assess the mechanism and reversibility of the process.

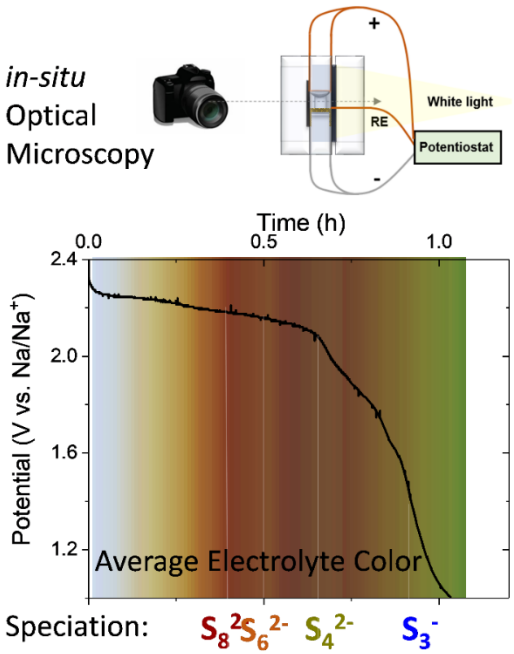

Fig 1- *In situ* optical microscopy diagnoses electrolyte color changes during the room temperature discharge of a sodium-sulfur cell. Reprinted with permission from ACS 2021.[13]

2. EXPERIMENTAL SETUP

2.1 Optical Cell Design

The *in situ* optical, electrochemical cell allows us to determine the reaction mechanism between sodium and sulfur in various electrolytes. The *in situ* cell, which we have used to demonstrate distinct lithium plating morphologies[14-15] and Li-ion overcharge behaviors,[16] here allowed us to correlate discharge voltages with intermediate polysulfide discharge products via their distinct colors.[17-18] For this analysis, the cell is modified to incorporate 3 electrodes, a sulfur cathode a sulfur cathode as working electrode (WE), adjacent a sodium metal counter electrode (CE) and sodium metal reference electrode (RE) (Figure 2A). The 0.25 cm gap between the working and counter electrode is filled with electrolyte, which is monitored *in situ*. The use of a 3-electrode configuration mitigated resistance effects from spatially separating the electrodes and enables electrochemical cycling at over several hours of operation. Viton o-rings in contact with quartz windows provide an airtight seal preventing oxygen and water contamination. The pixels between the sulfur cathode (WE) and sodium CE in each photo acquired were assessed and averaged for the entire electrolyte gap between electrodes to detect and analyze speciation

changes (Figure 2B). A sodium RE was included in contact with the electrolyte but not visible in the gap between the working and counter electrodes.

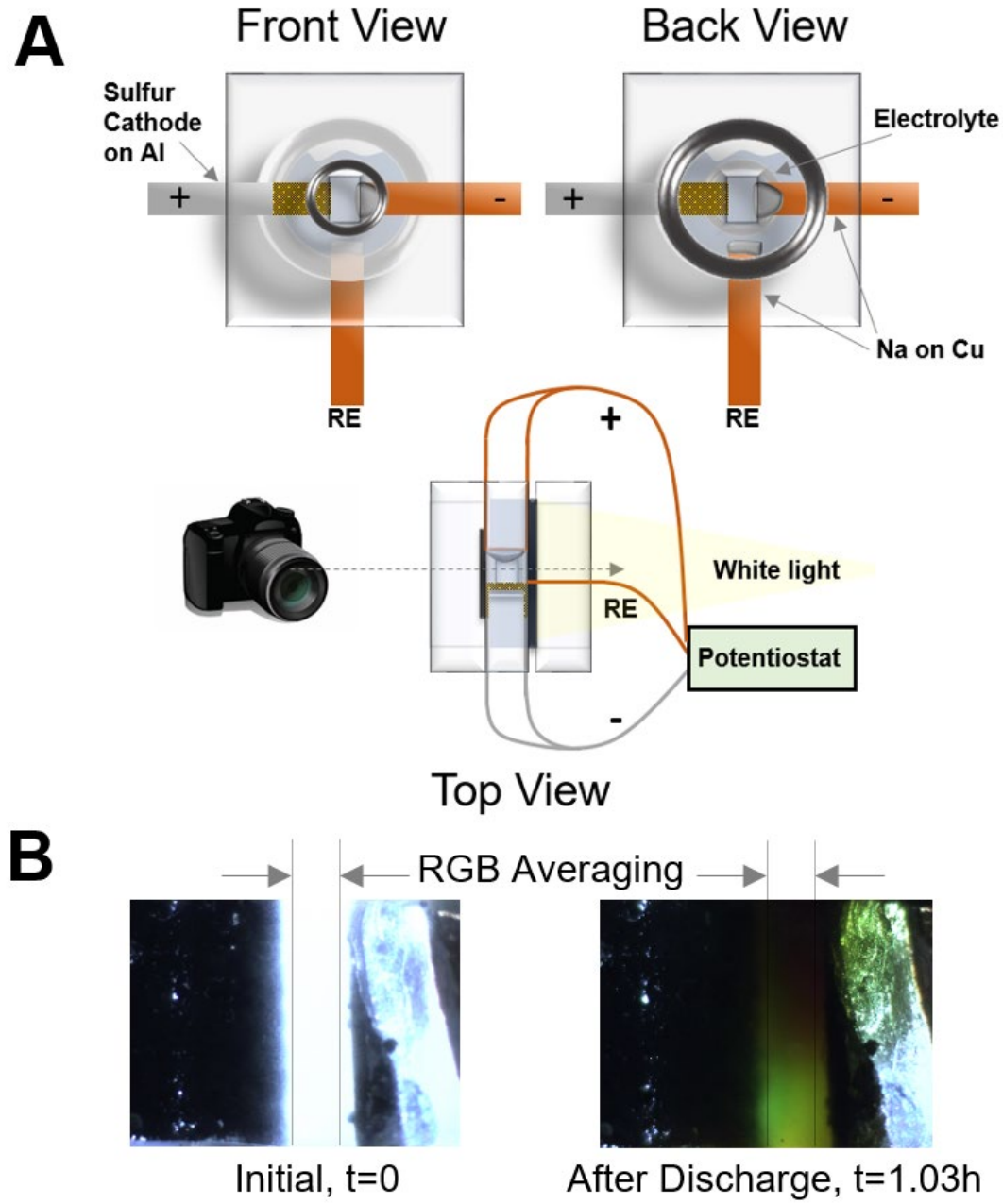

Figure 2- A Schematic representation of the optical, electrochemical *in situ* cell, **B** the electrolyte filled gap between the sulfur cathode (left) and sodium anode (right) where RGB pixilation is assessed. Two cases are shown: the initial case, when the electrolyte is colorless, and at the completion of a discharge, where various polyanions are present.

2.2 Sulfur Cathode Fabrication

A sulfur cathode was produced by melt infiltration of sulfur (S, sigma Aldrich, 99.99%) with carbon nanotubes (CNT, cheap tubes: 8-15 nm diameter multiwalls). The materials were hand mixed at a ratio of 60:40 S:CNT by mass and then vacuum-sealed into an ampoule. The ampoule was heated to 155°C for 12 hours to obtain a melt infiltrated S@CNT composite. The S@CNT material was cast into a slurry on 19 μm Al foil (MTI) with carbon black (CB, MTI) and carboxymethyl cellulose (CMC, Sigma Aldrich) at a ratio 80:10:10 S@CNTs:CB:CMC. The slurry was vacuum dried overnight at 60°C.

2.3 Polysulfide Solution Preparation

1M $NaPF_6$ solutions of G1 (dimethoxyethane, sigma adrich 99.95%), G2 (diethylene glycol dimethyl ether, Sigma Aldrich 99.95% anhydrous) and G4 (tetraethylene glycol dimethyl ether, Strem 99.9%) were prepared after vacuum drying the $NaPF_6$ salt (Strem, 99.95%) at 100°C and molecular sieve solvent dehydrations. Aliquots of these solutions were used to produce solutions of polysulfides by adding stoichiometric quantities of purified sulfur (S_8) and Na_2S (Strem, 99.95%).

2.4 *In situ* Optical Cell Experimentation

In situ optical microscopy was performed using a custom-made cell sealed in an argon-filled glovebox. For the cathode or WE, a strip (0.5 cm × 10 cm) of sulfur was cast onto aluminum. The anode consisted of a 0.5 cm × 0.5 cm coating of sodium metal (Sigma Aldrich) pressed onto the midline of a 0.5 cm × 10 cm × 25 μm strip of bare copper metal (All Foils; 99.999%) to form CE. The two electrodes were fed through a 0.25 cm × 0.5 cm opening in a plastic plate and pulled taut opposite each other. An additional piece of copper metal (0.5 cm × 5 cm × 25 μm) with metallic sodium at one end, was aligned inside the 010 Viton O-ring but below the opening in the plastic plate. This serves as the reference electrode (RE). Space was allowed between all electrodes to prevent shorting. Back and front plates with 1-in diameter quartz windows were placed on either side of the sample plate and separated by 006 Viton O-rings. Nylon bolts were used to hold the assembly in compression. Liquid electrolyte (~ 1 mL of 1 M $NaPF_6$ in G1, G2, or G4) was injected into the open cavity of the optical cell using a needle syringe. The cell was galvanostatically discharged to allow Na^+ transport and conversion at the sulfur cathode. Electrode surfaces and the gap between them were photographed with a Lumenera Infinity camera with Navitar Zoom 6000 lens assembly during charging. Electrodes were imaged at 3.38× magnification with a resolution limit of 7.7 μm. The gap was also assessed with UV-vis.

2.5 Image Processing

Image processing and analysis was completed through the implementation of a Java computer program, written to process hundreds of images at a time. For each image, the script first isolated the electrolyte present in the optical cell from the two electrodes by using a basic form of edge detection. The edges were set based on the relative change of RGB values in adjacent pixels. When this ratio changed by greater than 75%, the program defined this as an

electrode edge. Once the location of the electrolyte had been determined, the program treated this part of the image as a 2-D array of pixels, with each pixel possessing a red, green, and blue value between 0 and 255. Scanning each pixel present in the electrolyte photo, the program calculated the average RGB value across the entire image, as well as the percentage that each color (red, green, and blue) contributed to the image as a whole. Each of these ratios corresponded to a particular time the photo was taken and allowed the researchers to judge the time at which each phase of the reaction took place. Additionally, the script constructed a linear mural by assembling images of the average RGB value for each electrolyte photographed. This provided a qualitative element to compliment the quantitative RGB analysis and displayed representative colors for the observer to visualize the colors present in each stage of the reaction.

3. EXPERIMENTS

3.1 Polysulfide Solution Analysis

The glyme solvents are chain-like and increase in length from G1 to G4. As they increase in length their number of oxygen molecules increases as well as their viscosity (Table 1). Since the electrolyte is initially colorless and the S_8^{2-} polyanion is dark red in color, the solubility behavior is readily visible.

Table 1- Material properties of glyme ether solvents at 20°C relevant to solubility and electrochemical performance.[1]

Glyme Properties at 20°C	Density (g/cm^3)	Molar Mass (g/mol)	Atomic Oxygen Ratio (atoms/molecule)	Volumetric Oxygen Ratio (10^{23} atoms/cm3)	Viscosity (mPa s)
G1	0.861	90.1	2	0.115	0.42
G2	0.938	134.2	3	0.126	0.98
G4	1.00	222.2	5	0.136	3.7

Polysulfide solubility in glyme electrolytes is enabled by Lewis base lone pair electrons at the oxygen molecules in the solvent chains.[19] Notably, despite the increase in number of oxygen atoms from G1 to G4, the density of these lone pairs in a volume remains approximately the same since their molar mass and density also increase from G1 to G4 (Table 1). Therefore, similar solubility is anticipated among the three electrolytes (G1, G2 and G4). However, it is also important to note that viscosity increases from G1 to G4, which plays an important role in ionic interactions. Lewis base lone pair density and solvent viscosity will influence solubility and tendency to facilitate reordering of solubilized species. To decouple electrochemical behaviors from solvent properties, we chemically produced Na_2S_8 in each of the electrolytes at known concentrations allowing us to assess solubility and tendency to stabilize radicalization ($S_3^{\bullet-}$) in natural chemical reordering.

Since sodium and sulfur spontaneously react when not phase separated, 0.1M stock solutions of Na_2S_8 were produced by stoichiometric mixing of sulfur and Na_2S in each of the 3 glymes: G1, G2, and G4. Aliquots from this solution were then added to 1M $NaPF_6$ electrolytes of the same glyme type to obtain specific concentrations of Na_2S_8. Figure 3A reveals photographs of 1, 2.5, 5 and 10 mM Na_2S_8 in each glyme electrolyte, spanning the range from

colorless to dark brown at 1cm optical and spectroscopic pathlengths. Optical detection of the polysulfides via yellow or brown coloration onsets abruptly. In G1 and G2 the solution remains colorless until 2.5mM Na_2S_8 and in G4 until 5mM Na_2S_8. Further, upon polysulfide detection, the solution rapidly becomes very dark (when molarity increases from 2.5 to 5mM Na_2S_8). At 5mM Na_2S_8 it is observed that as the glyme chain length increases from 1 to 4, the solution appears darker, indicating solubility increases.

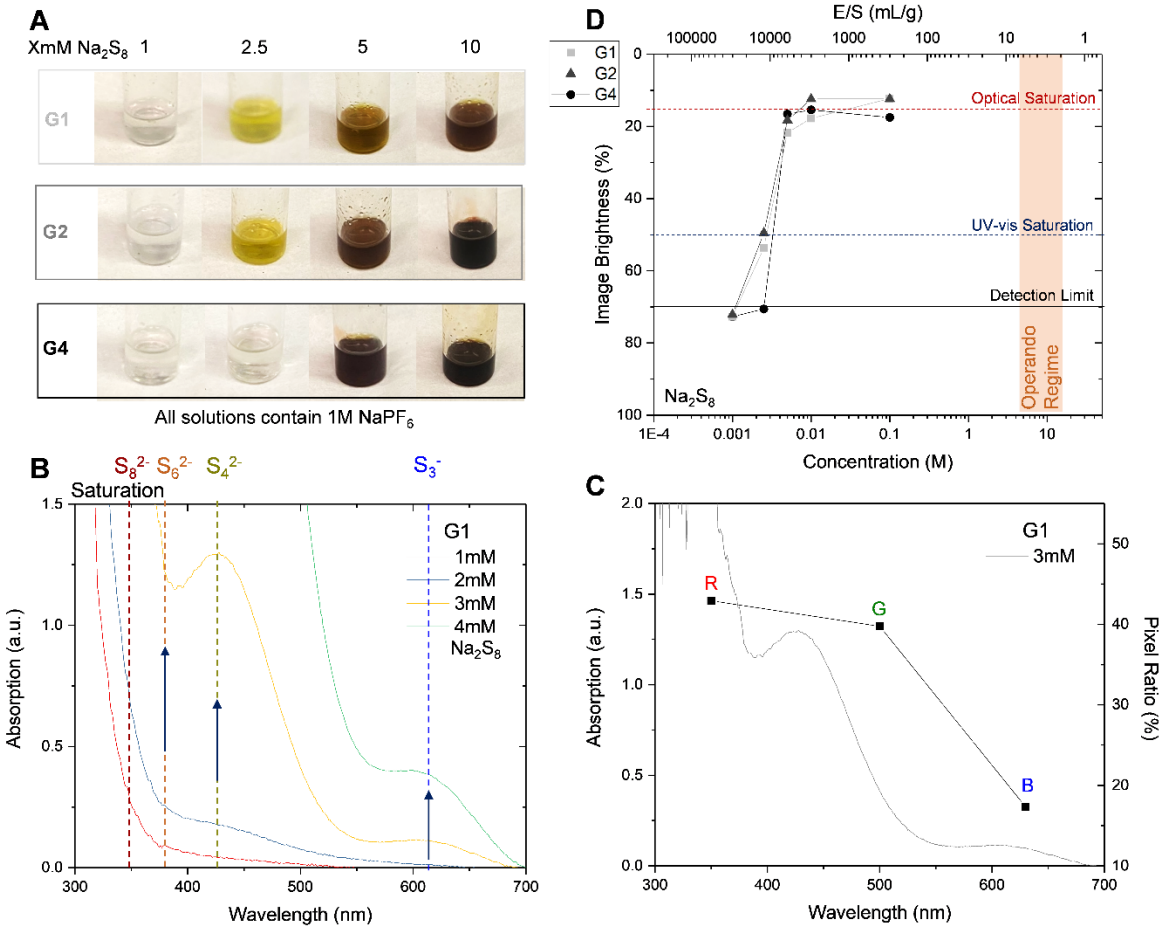

Figure 3- A Photographs of Na_2S_8 solutions of increasing concentration from left to right (1, 2.5, 5 and 10 mM) in glyme based electrolytes containing 1M $NaPF_6$; solutions are ordered by increasing solvent chain length from top to bottom (G1, G2 and G4). **B** UV-Vis spectra of 1M $NaPF_6$ G1 solutions containing increasing concentrations of Na_2S_8; the approximate absorption wavelength of polyanions of interest are indicated with color coded dashed lines. **C** Average RGB pixel ratio (right y) in a photograph of 3 mM Na_2S_8 in 1 M $NaPF_6$ G1 overlaid with the UV-Vis spectra from the same solution (left y). **D** Average image brightness through solutions of increasing concentration (log scale) of Na_2S_8 in G1 (light grey), G2 (dark grey), and G4 (black) electrolytes. Concentration is converted to a theoretical electrolyte to sulfur ratio (E/S) assuming all elemental sulfur solubilizes during a discharge and is shown on the top x-axis. The detection limit of each measurement (optical and UV-Vis) when the solutions appear colorless is indicated with a solid black line, saturation of the UV-Vis detector with 1 cm pathlength is indicated with a blue dashed line, and optical saturation with the same pathlength is designated with a red dashed line. Reprinted with permission from ACS 2021.[13]

In this Na_2S_8 concentration regime (1-10mM), where optical comparison of solutions reveals a strong dependence of coloration on concentration, UV-Vis spectroscopy is performed to determine if these color changes simplistically detect changes in solvent/polysulfide ratio or if these ratio changes spur chemical reordering. In G1, the glyme with evidence of the lowest polysulfide solubility (Figure 3A), the ratio of polysulfide types in solution is assessed as concentration is increased from 1 to 4mM of Na_2S_8, through a pathlength of 1cm (Figure 3B). The absorption wavelength associated with the sulfur polyanions of interest are indicated with color-coded dashed lines (S_8^{2-} red and ~350nm, S_6^{2-} orange and ~380nm, S_4^{2-} yellow and ~420nm, and $S_3^{\bullet-}$ blue and ~610nm). At 1mM Na_2S_8 there is minimal detection (<0.3a.u.) across the range of interest (350-700nm), which agrees with the optical findings at 1mM in Figure 3A (colorless). Subsequently mild increases (~0.2a.u.) in absorption are observed at 2mM with some increase at the S_8^{2-}, S_6^{2-}, and S_4^{2-} regions. However, when the concentration increases to 3mM, absorption is dramatically enhanced and saturates detection below 400nm preventing relative quantification of S_8^{2-} and S_6^{2-} species. A strong S_4^{2-} absorption is observed and a mild presence of S_3^- is detected. It is known that the S_4^{2-} polyanion is yellow[19] and the 2.5mM solution of Na_2S_8 in G1 appeared yellow in Figure 3A. However, with saturation at the expected S_8^{2-} red-brown wavelength (~350nm), UV-Vis cannot diagnose the yellow color as S_8^{2-} disproportionation into $2S_4^{2-}$ or dilution (ratio of solvent to species), despite the low concentration. Finally, at 4mM Na_2S_8, absorption saturates for all wavelengths below 500nm. Therefore, we detect enhanced $S_3^{\bullet-}$ absorption compared to the 3mM solution, but cannot compare its response to the other polyanions at 4mM due to saturation of the detector at wavelengths where the other polyanions would be detected. At 4mM Na_2S_8 the solution is brown in color, similar to 5mM Na_2S_8 in G1, shown in Figure 3A.

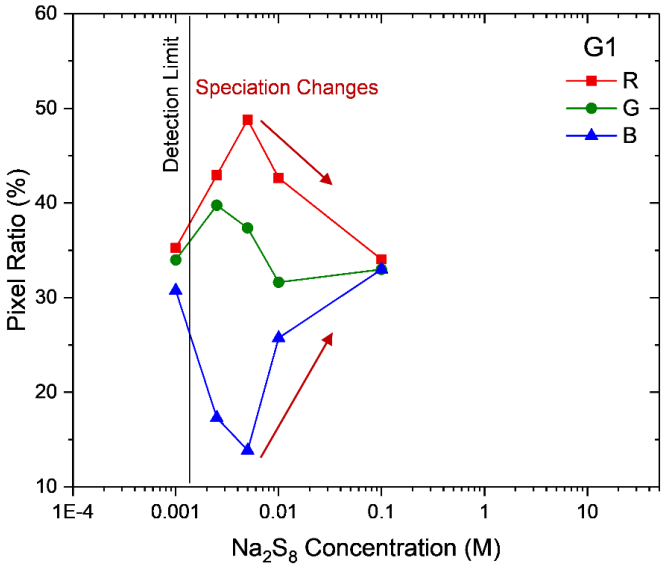

Figure 4- RGB pixel ratios in solutions of increasing concentration (log scale) of Na_2S_8 in G1 1M $NaPF_6$ electrolytes.

Since the regime between detection and saturation of polysulfide anions in UV-Vis remains quite small (1-4mM in G1), the technique is not practical for *in operando* analysis of the system. Even if pathlength is substantially reduced, a specific concentration would need to be

targeted by *in situ* experimentation, and this concentration would also vary for each glyme since their solubility also varies. Therefore, we calculate the RGB ratios correlating to red, green and blue pixels from the photographed Na_2S_8 solutions of various concentration in G1 (Figure 3A) in Figure 4 to determine the viability of this technique for determining speciation. In direct comparison to the 3mM UV-Vis spectra in Figure 3C, RGB pixel ratios indicate similar color dominance to the higher resolution UV-Vis spectra when R, G, and B are aligned with their approximate absorption wavelengths.

For each pixel, three numbers with values from 0 to 255 (opaque to transparent) are used to dictate the image color and intensity; here, the ratios are used to isolate dominant colors. At 3mM the values are 167, 161, and 60, respectively, resulting in ratios of 43, 41.5, and 15.5%. The ratios are used to assist in visualizing relative change in color over time. Despite only providing 3 color specific values per measurement, compared to the high resolution (1/nm) delivered by UV-Vis, these three values enable effective assessment of soluble polysulfides, since desirable polyanions are red in color (S_8^{2-}) and undesirable are blue ($S_3^{\bullet-}$) and coexistence of both types appear green. Again, in attempt to determine if speciation is concentration dependent, various concentrations are assessed for RGB pixilation (Figure 4). In colorless solutions (1mM Na_2S_8 in G1) the RGB ratios approach unity (33.3% each). As the concentration increases to 5mM Na_2S_8 in G1, R and G increase while B decreases, agreeing with the UV-Vis trends seen in Figure 2B. With further increase in concentration, R and G decrease and B increases. This is likely evidence of enhanced chemical disproportionation into the blue $S_3^{\bullet-}$ radical at higher concentrations, which was not diagnosed with UV-Vis, since the detector saturated in the red regime with concentrations higher than 2.5mM. This trending follows from 10mM to 100mM, where the solution becomes very dark and the RGB ratio again converges close to unity; here at full absorption as opposed to reflection (1mM Na_2S_8, colorless).

The transition from colorless (average pixel value 255) to optically saturated (average pixel value of 0) can be assessed using the image brightness as demonstrated in Figure 3D with a white image providing 100% brightness and black, 0%. Here, the brightness levels of the photographs in Figure 3A were characterized with G1 solutions indicated by light grey circles, G2 by grey triangles, and G4 by black circles. With a 1cm path length, UV-Vis analysis saturates at ~50% image brightness, which is labeled by a navy dashed line, excluding most of the solution concentrations that we prepared from effective UV-Vis analysis. With the same pathlength, RGB pixilation can be assessed to as low as ~15% brightness (~10mM Na_2S_8 in G2 in Figure 3A), allowing the technique to span a wider concentration regime. Further, we convert each concentration to a relevant electrolyte to sulfur ratio (E/S), assuming all active sulfur dissolves into solution during conventional battery operation. Therefore, an *operando* regime falls between 3 and 11 M which correlates to E/S ratios between 8 and 2 mL/g.[8] Our prepared solutions do not fall in this regime, since these concentrations are near solution saturation,[17] but the E/S ratio in our optical cell may be tailored to approach *operando* conditions. Herein we utilize an E/S ratio of ~1000 mL/g, which is 2.5 orders of magnitude higher than a viable E/S ratio for UV-Vis analysis (50,000 mL/g) in the same test fixture. Since optical analysis can probe much higher polysulfide concentrations than UV-Vis spectroscopy, the path length or gap between electrodes in an *in situ* cell may be tailored for *in operando* analysis, while maintaining the distinct advantage of facilitating investigation of sodium metal morphologies and other critical mechanisms simultaneously. This assessment indicates that simplistic optical analysis of image brightness and RGB pixilation can bridge a wide range of solution concentrations, providing superiority to UV-Vis spectroscopy.

3.2 Discharge Mechanism

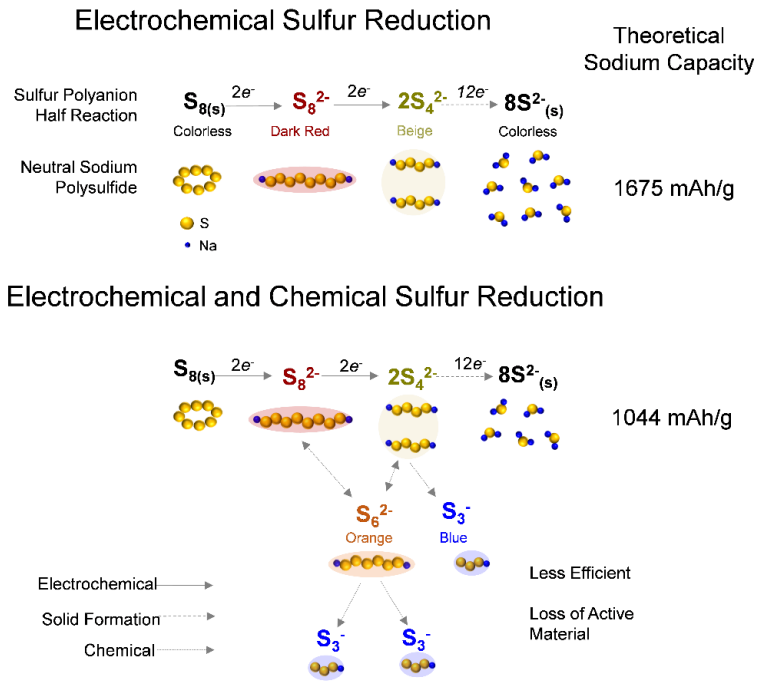

Figure 5- Schematic comparisons of the desired electrochemical sulfur reduction to electrochemical and chemical sulfur reduction, including cathodic half reactions and neutral discharge products. Sodium ions are color coded blue and sulfur is yellow. Electrochemical processes are indicated with a solid line, solid precipitation with a dashed line, and chemical reordering with a dotted line. Elements that are soluble in the system's electrolyte are color coded with the color they turn the usually colorless solution. Reprinted with permission from ACS 2021.[13]

Much like the analogous Li-S system prior to electrochemical cycling, the Na-S system begins with elemental sulfur at the cathode isolated from metallic sodium by colorless electrolyte. In ambient conditions, sulfur crystallizes in cyclo-octasulfur molecules (S_8). During electrochemical reduction or discharge, the S_8 molecule is reduced to S_8^{2-} as 2 Na^+ ions break the ring structure, forming a neutral chain with Na^+ at each extremity. This long chain polysulfide is highly polar with positive charges concentrated at small Na^+ ions and negative at large ionized sulfur chains. The polarity facilitates complexation between the Na^+ ions and the oxygen molecules in the glyme solvents which possess Lewis base electron lone pairs.[20]

The long chain polyanions are broken into shorter chains as the sulfur is further reduced and more sodium ions are introduced. With further electrochemical reduction the second product is the beige S_4^{2-}, which is the smallest soluble polyanion. Therefore, with subsequent electrochemical reduction, the high energy Na_2S solid is nucleated at the cathode, leaving the electrolyte colorless again upon complete conversion. This solid nucleation accounts for ¾ of the theoretical discharge, since 12e⁻ are released per 1 original S_8 molecule. Therefore, under an

applied constant current, reduction and solid nucleation will be slow compared to the reduction of the longer chain, soluble polysulfides occurring in solution at the beginning of the discharge.

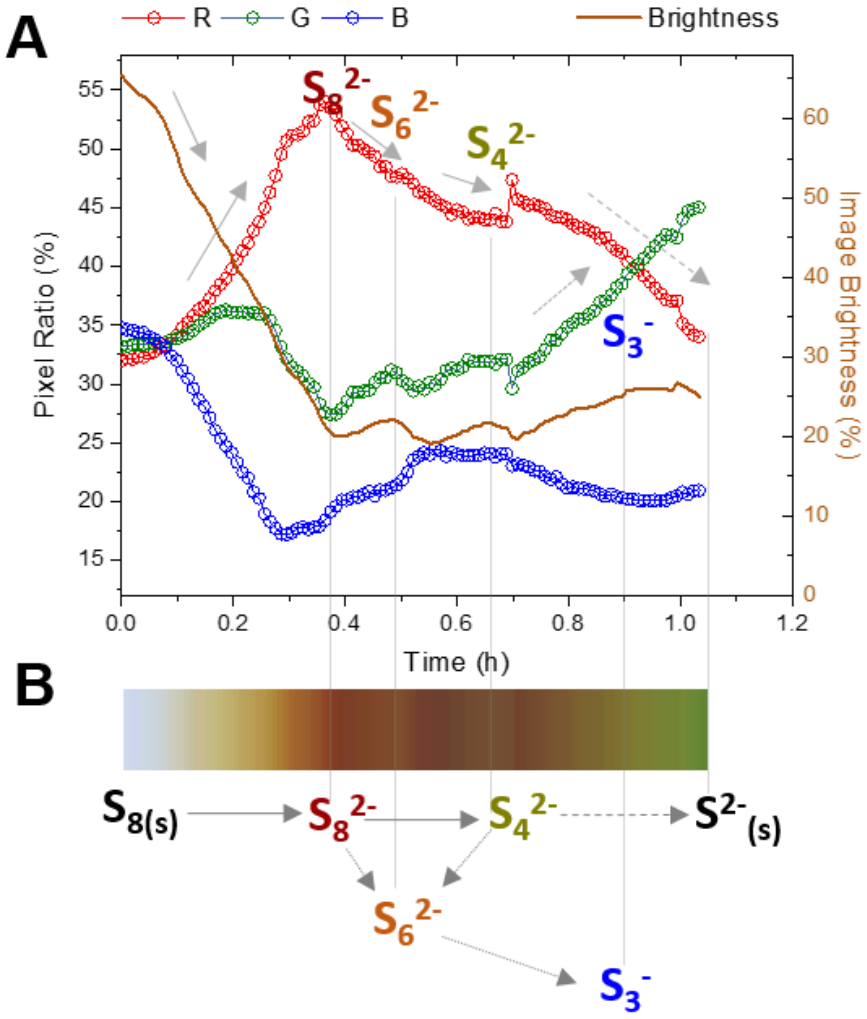

Figure 6- A Representative RGB pixilation assessment over time, including pixel ratios (left y-axis) and image brightness (right y-axis and golden in color). Evidence of distinct polyanions are indicated with notation, color coding, and arrow type agreeing with Figure 1. **B** Color bar indicating the electrolyte's average color over time aligned with the cathodic half reactions from Figure 1. Reprinted with permission from ACS 2021.[13]

If the solution permits, solubilized polysulfides may disproportionate and recombine. In this case other polysulfides including S_6^{2-} (orange) and $S_3^{\bullet-}$ (blue) may form. This hinders the desired electrochemical pathway, dropping the theoretical specific capacity by ~38%.[19] The $S_3^{\bullet-}$ radical ion is particularly undesirable, since it disrupts the conventional 2e- transfer charge balance. This causes it to remain in the electrolyte as lost active material, as visualized in the electrochemical and chemical sulfur reduction portion of Figure 5. Since the final reaction step to nucleate solid $8S^{2-}$ (Na_2S) accounts for ¾ of the reaction time, it is likely to observe disproportionation and recombination at this time while the soluble species await solid nucleation.

Each intermediate sulfur polyanion exhibits a distinct visible color, as indicated by color coding in Figure 5. Notably, if a 2^- polyanion radicalizes to $1^{\bullet-}$, it is characterized by a color change from red to blue in the visible spectra (~700 nm to ~450 nm).[21-22] This substantial difference in visible color allows broadly accessible optical microscopy to be as effective as the popular UV-Vis spectroscopy in identifying undesirable radicalization of the solubilized polysulfides in various electrolyte solvents, as discussed in depth in part 3.1.

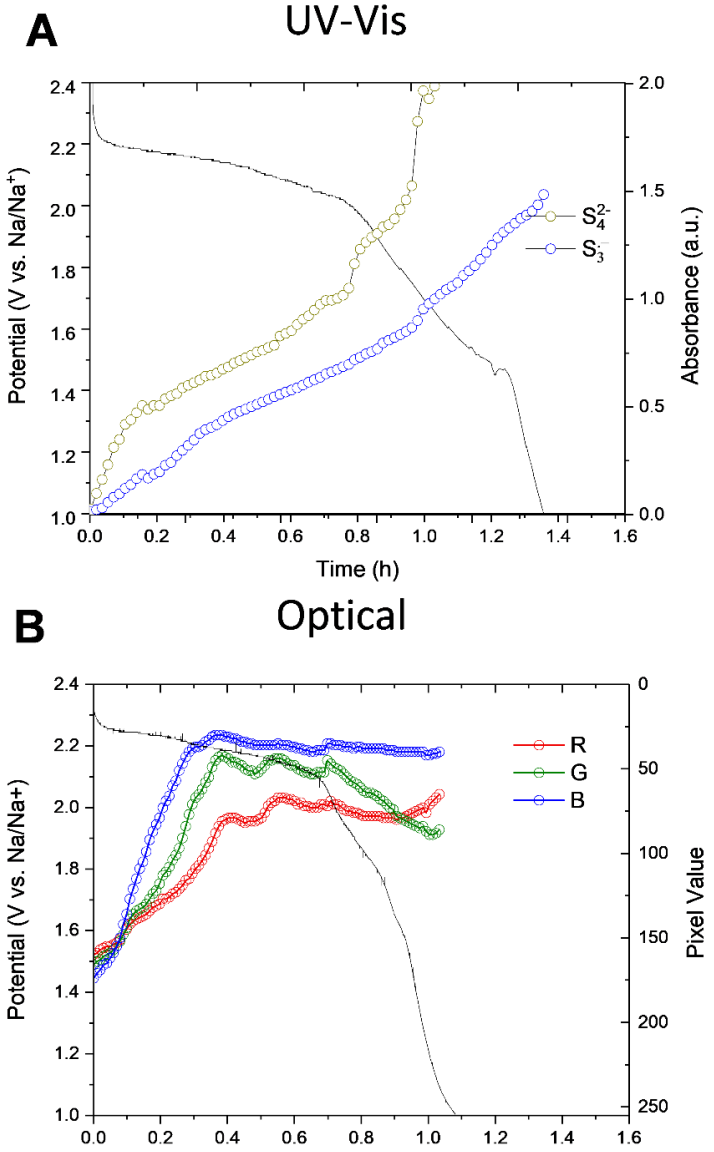

Figure 7- Voltage during C/2 galvanostatic discharge in G2 (left y) and (**A**) absorption at wavelength associated with S_4^{2-} and $S_3^{\bullet-}$ (Figure 2B) acquired through the electrochemical *in situ* cell (Figure 3A). **B** A different electrochemical cell's voltage during C/2 galvanostatic discharge in G2 (left y) and the correlated raw RGB pixel values.

Using RGB image of the electrolyte gap in the *in situ* cell (Figure 2), evidence of poyanion chain -length reduction (decrease in R) and radicalization (increase in G and B) is

observed. The pixels between the sulfur cathode and sodium counter electrode in each photo acquired are assessed and averaged for the entire electrolyte gap between electrodes to detect and analyze speciation changes (Figure 6A). The raw pixel values (3 numbers correlating to RGB pixel saturation) over time are directly compared with changes in the S_4^{2-} and $S_3^{\bullet-}$ absorption over time detected with UV-Vis measurements through the same electrochemical cell subjected to the same discharge conditions, with discharge current expected to deliver a 2 hour discharge(0.2 mA or C/2 in G2) Figure 7. The R pixel most closely compares to the S_4^{2} ions tracked with UV-Vis, but also detects the S_8^{2-} which is not accessed with UV-Vis measurement. The B pixel detects the $S_3^{\bullet-}$ and the G detects the yellow S_4^{2-}, especially in the presence of the blue $S_3^{\bullet-}$. In both experiments, increased detection of color is observed over time, with increased absorption in UV-Vis and decreased pixel value or image brightness in optical analysis. However, in the UV-Vis assessment, the relative presence of each species cannot be assessed beyond 1 hour of discharging, as the detector saturates (Figure 8), and S_8^{2-} (low wavelength absorption) is difficult to assess at all. Alternatively, RGB pixel assessment is stable over the entire measurement, and clear relative pixel changes and inflection points are detected. Therefore, to more intuitively visualize and track solution color changes during a discharge optically, pixel ratios and percentage brightness are calculated from each image collected (Figure 6A). In order to explain how this data is used to track the sodium sulfur discharge mechanism, exemplary optical data from a C/2 discharge in G2 is shown in Figure 6A.

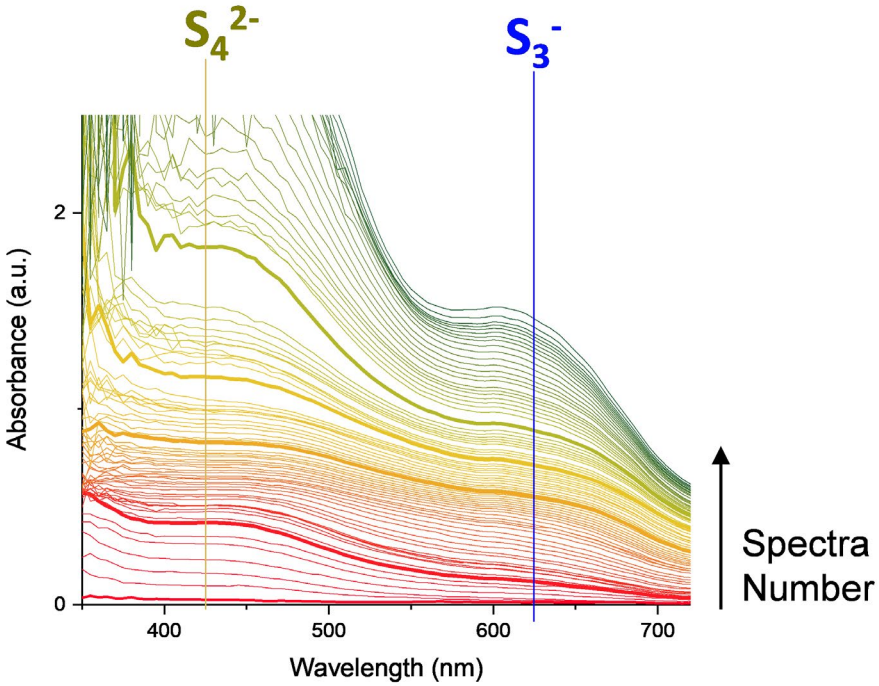

Figure 8- Full UV-vis spectra from Figure 7A collected ~every 2 minutes. Each spectra is color coded with approximate visual color of the electrolyte solution.

Initially, when the cell is assembled, representing a charged condition, the electrolyte is transparent (image brightness >60% and RGB ratio at ~unity). As the discharge begins, the

electrolyte begins to turn a red-brown color, causing the R content to increase, while B and G decrease. This continues until the electrolyte becomes very dark (~20% brightness), and the red pixel reaches a peak at ~55%, after 0.38h. Here, the sulfur from the cathode has reduced to S_8^{2-}.[23] As the reaction continues, the solution becomes less visually saturated (apparent by fluctuations in brightness), as the S_8^{2-} anions in solution reduce further to the yellow S_4^{2-} anions. During this reduction, R decreases and B and G increase owing to the coversion of the red polyanion (S_8^{2-}) during this process. There are two valleys in the brightness at 0.48 and 0.66h, respectively, which correlate to peaks in B and G pixel ratios. These features are correlated to the detection of S_6^{2-} and finally S_4^{2-} polyanions, in that order. This provides evidence that the glymes will allow chemical reordering, since electrochemical reduction alone would not produce S_6^2. As depicted in the electrochemical reduction of sulfur in Figure 5, following the reduction to S_4^{2-}, the soluble anions should reduce and precipitate into the solid S_2^{2-} (Na_2S), which would cause the electrolyte to return to colorless, but only if the precipitation is complete. When chemical reordering is facilitated in tandem with the electrochemical reduction of sulfur, some polyanions, especially $S_3^{\bullet-}$, will remain in solution when the cutoff voltage is reached. Since this final step of the reaction to form Na_2S requires solid nucleation and occurs over a longer time scale (3/4 of the discharge time), chemical reordering of polyanions awaiting precipitation from solution permits formation of the $S_3^{\bullet-}$ polyanion, which does not have a direct path for electrochemical reduction into Na_2S (Figure 5). Therefore, in this region as the R pixel and brightness decrease, the G pixel increases; the radical $S_3^{\bullet-}$ forms in the presence of the yellow S_4^{2-}, producing a bright green hue. From the average of RGB pixel values in the electrolyte region of the *in situ* cell (Figure 2B), an average color can be generated. In this manner, a color bar representing electrolyte color over time is achieved (Figure 6B). Aligning this color bar with the brightness and pixel ratio trending assists in the identification of the discharge mechanism, predicted beneath the electrolyte color in Figure 6B.

3.3 Solvent Comparison

To demonstrate the ability of this technique to draw comparative conclusions, the discharge mechanisms in G1, G2 and G4 were assessed, enabling the presence of distinct polysulfides to be assigned to cell voltages, allowing the support of the conversion reaction to be compared (Figure 9). Beginning with G1, the shortest chain glyme ether, the discharge voltage is constant for the first 0.4 h (Figure 9A) as the S_8^{2-} polyanion forms. Here, the relative R pixilation increases and brightness decreases (Figure 9B), behavior consistent with an increase in S_8^{2-} concentration. Subsequently, the yellow S_4^{2-} is formed from 0.4-0.7 h as indicated by a relative decrease in R pixelation and increase in image brightness. The brightness peaks, as the initial voltage plateau terminates. From this point, until the lower voltage cutoff is reached (1V), the soluble species are converted to solid discharge products. Since the reaction kinetics slow for nucleation of the solid Na_2S product,[4] the sulfur radical ($S_3^{\bullet-}$) is detected and its concentration grows until test completion, as indicated by the relative B and G pixelation surpassing R, combined with the gradual decrease in image brightness. During this portion of the reaction, two plateaus are detected in the discharge, likely correlating to formation of solid Na_2S_2 and Na_2S, respectively. However, optical image analysis alone cannot confirm this assertion, since Na_2S_2 and Na_2S are both solid products produced at the cathode, removing color from the electrolyte. Notably, over the duration of the reaction (in G1), the image only darkens ~40% and the pixel

ratio fluctuates only ~5%. Looking at the color bar (Figure 9C), we see that the average color remains close to transparent over the entire discharge, and by viewing the cell at the completion of the reaction (Figure 9D), we can see that the soluble products that remain are close to the sulfur working electrode. Looking at the acquired photographs over time reveals that the species remained close to the sulfur cathode through the duration of the discharge. This behavior enabled ~72% of the theoretical discharge capacity in G1, despite evidence of sulfur radicalization, suggesting that electrochemical reactions dominate chemical reordering in G1.

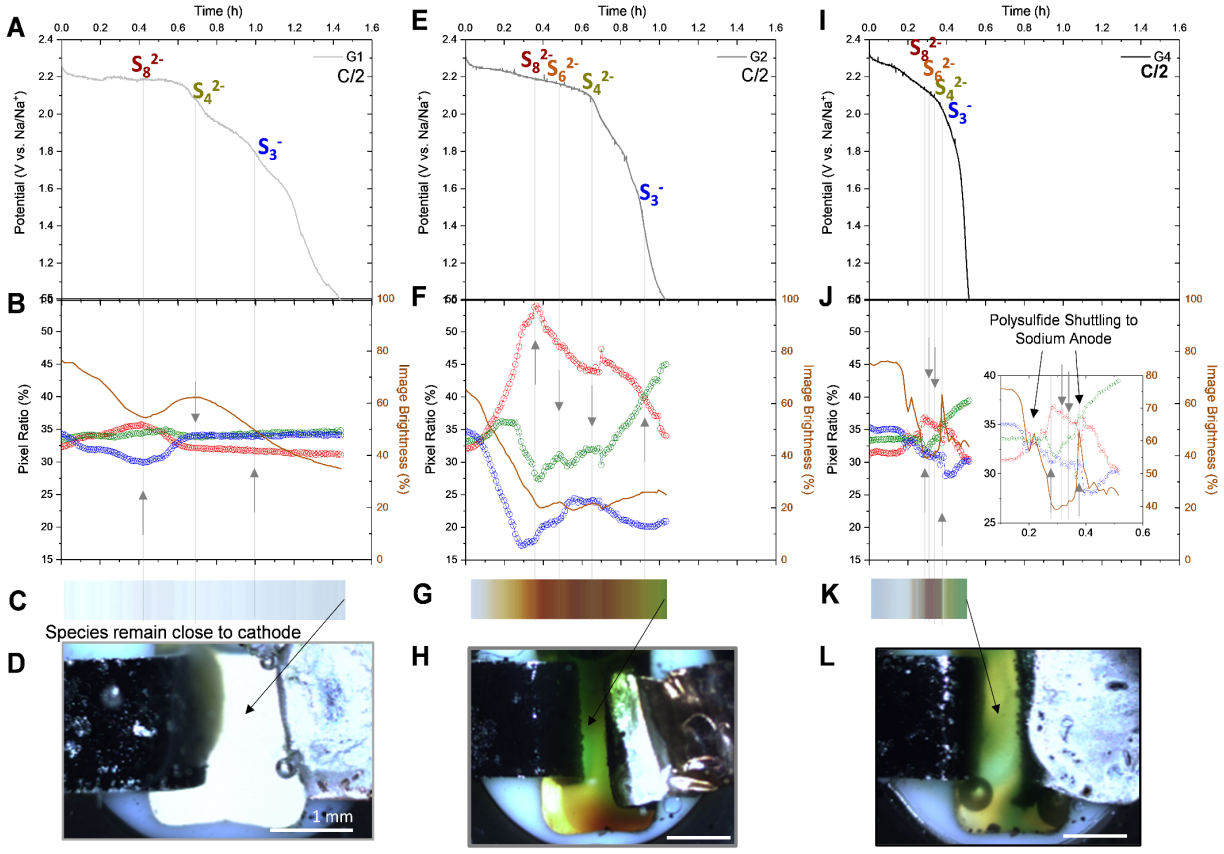

Figure 9- Electrochemical and optical analyses of discharge in G1 (left column), G2 (center column), and G4 (right column). **A, E, I** Voltage during C/2 galvanostatic discharge, **B, F, J** RGB pixel analysis including pixel ratio and image brightness aligned with discharge voltage, and **C, G, K** the resulting average electrolyte color bar. Distinct changes in electrolyte color are indicated with grey vertical lines and notated with the polyanion responsible for these changes. **D, H, L** Photographs of the optical cell window at completion of the electrochemical discharge. Reprinted with permission from ACS 2021.[13]

Next, in G2, the exemplary data discussed in Figure 6 and 7, a shorter discharge and therefore lower discharge capacity than G1, is achieved. However, the first voltage plateau terminates after approximately the same duration of discharge for G1 and G2 (~0.6h). The

disparity in their behavior following the first plateau is a result of substantially more disproportiation in G2 (Figure 9E). This enables the distinct detection of S_6^{2-} in the soluble regime or first voltage plateau, preceding evidence of $S_3^{\bullet-}$ when the reaction kinetics slow at the plateau's termination. G2 ultimately facilitates only ~52% of the theoretical discharge capacity due to the less direct reaction path. The image analysis (Figure 9F) and color bar (Figure 9G) reveal substantially more electrolyte coloration and less brightness than in G1 (pixel fluctuations of 40%), which agrees with the prediction made from stoichiometric solutions (Figure 3A and D) in which higher polysulfide solubility is enabled in longer chain glymes. Figure 4H shows the cell at the completion of the discharge and reveals that $S_3^{\bullet-}$ radicalization (evinced by electrolyte turning green) is most prominent between the working and counter electrode, while high order polysulfides that are dark in color, like S_8^{2-} and S_6^{2-} have sunk to the bottom of the cell. The latter enhances loss of active material, truncating the discharge capacity. Although this is an effect of the cell geometry used for *in situ* investigation and does not directly translate to practical operation, it reveals that G2 is prone to polysulfide shuttling, which causes capacity loss.

A replicate of the G2 experiment is provided in Figure 10A and 10B demonstrating similar discharge behavior and a subsequent charge of the remaining active material. During the charge, the conversion process is reversed to reform sulfur at the cathode or WE and plate sodium at the CE. As anticipated, in the reversal, evidence of S_4^{2-} speciation precedes S_8^{2-}, reversing the chronology of discharge. The efficiency of the cycle is low, since substantial active material was lost in discharge, and it is difficult to decouple the reaction reversal at the cathode (WE) from sodium plating at CE. However, valuable mechanistic understanding is gained from the analysis of the discharge. The voltage profiles of two additional experiments are shown in Figure 10C and 10D to demonstrate the repeatability of the experiment.

Finally, in G4, a rapid discharge is observed (Figure 9I) with the lowest discharge capacity of the electrolytes tested. Despite the short reaction, image analysis (Figure 9J) reveals similar discharge mechanisms to G2. When S_8^{2-} peaks at 0.3 h, indicated by a peak in relative R pixilation and minima in image brightness, S_4^{2-} begins to form, indicated by decreasing brightness and R. The inset of 4J reveals that, in this region following the peak of S_8^{2-}, similar trending of B, G and brightness seen in the G2 analysis (Figure 9F) are observed, just over a much shorter timescale. This finding, and the shortened timescale, emphasize the propensity for the polyanions to reorder in G4. Subsequently, R continues to decrease but B and G increase, indicating $S_3^{\bullet-}$ radicalization. During this discharge, two sharp increases in image brightness are observed (at 0.22 and 0.38 h), which correlate to light regions of the color bar (Figure 9K). Examining the acquired photos in succession, we can see that the dissolution of sulfur into soluble products proves somewhat violent, causing turbulent mixing in the cell, which is also apparent at the completion of the reaction (Figure 9L). This behavior rapidly dissipates active material, causing the temporary brightness or transparency in the cell and facilitating the brief, low capacity discharge.

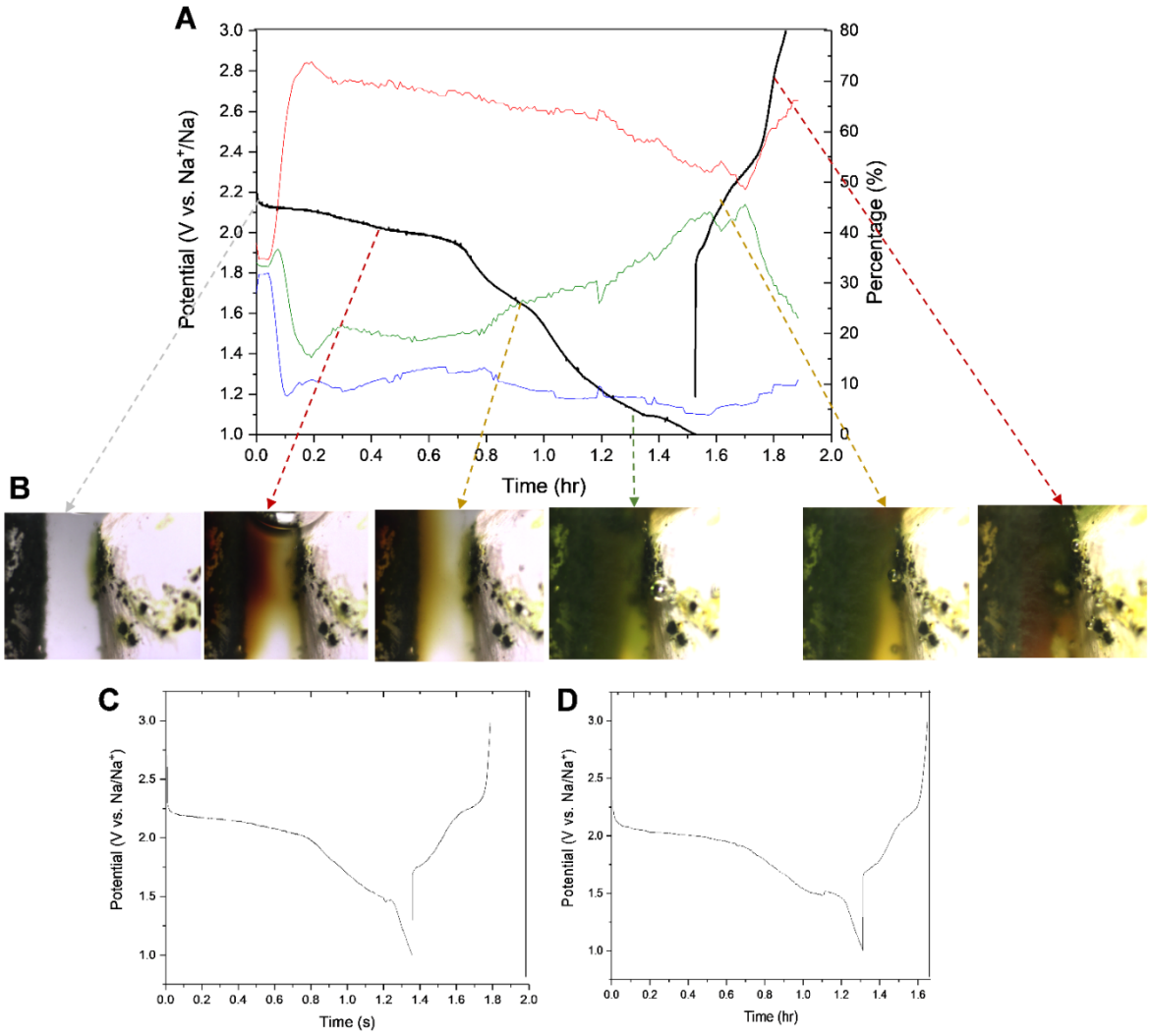

Figure 10- A Voltage during C/2 galvanostatic discharge and subsequent charge in 1M $NaPF_6$ G2 electrolyte (left y) and RGB pixel ratio (right y). **B** Photographs of optical cell revealing electrolyte color change at key voltage points during the discharge and subsequent charge. Arrows indicate approximate color. **C** and **D** Replicates of **A**.

3.4 Temperature Variation

When solutions were synthesized and tested, warm solutions took on a green hue, indicating an increase in undesirable radicalization to S_3^- ions. Therefore, UV-vis analysis of polysulfides (2mM Na_2S_8) in electrolyte solutions, 1M $NaPF_6$ in G2, was completed, as the solution was heated from 0 to 50°C. Photographs of the cuvettes at 0 and 50°C are shown in Figure 10A, revealing a visible color change from mustard yellow to light green. Figure 10B shows the UV-vis spectra acquired during the cuvette heating. The solution initially only shows evidence of S_4^{2-} ions over the region probed (350-700nm). As the solution was heated, the absorption in the S_4^{2-} region (400-500nm) of the spectra decreases and a peak in the S_3^- radical

region (550-700 nm) appears and grows. This result emphasizes that increasing solution temperature permits radicalization of polysulfide anions.

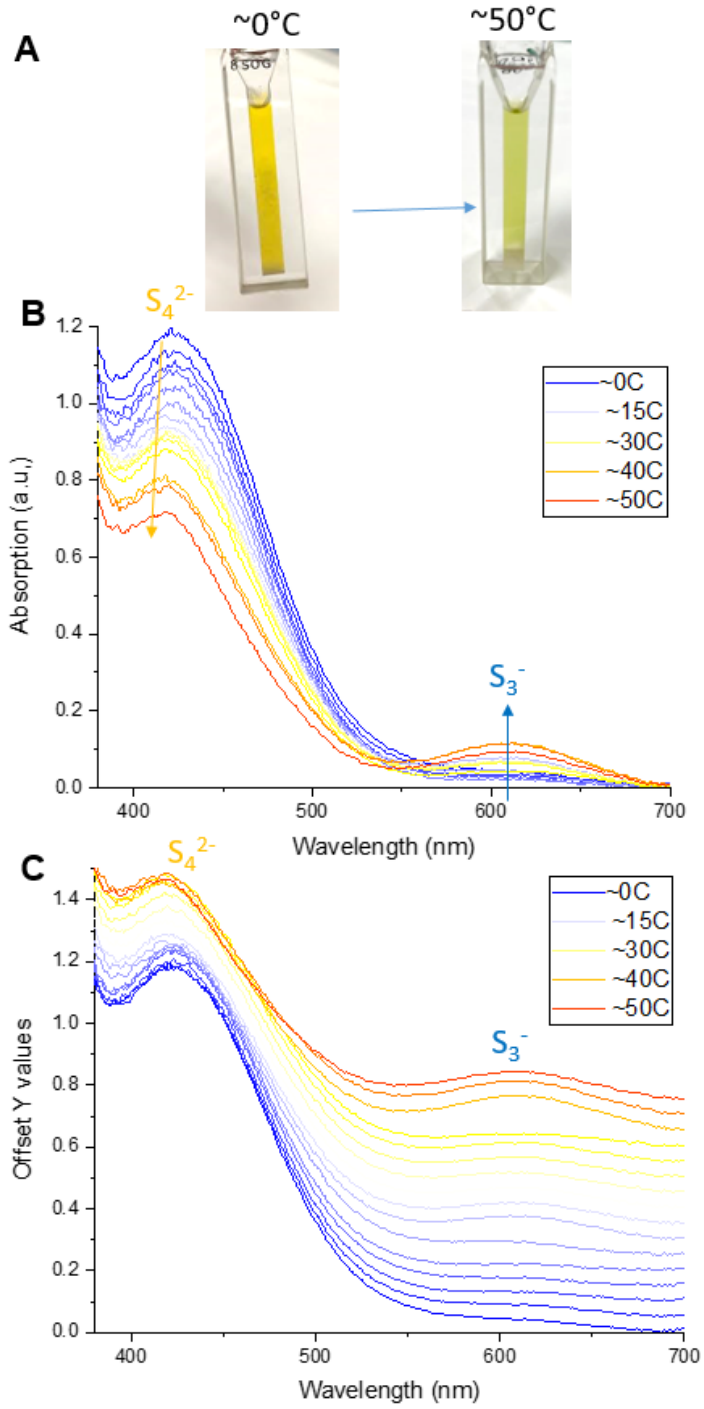

Figure 10- A Photographs of quartz cuvettes containing 2mM Na_2S_8 added to solutions of 1M $NaPF_6$ in G2 at 0 and 50°C. **B** UV-Vis spectra obtained as the cuvette in **A** was heated from of 0 to 50°C. The yellow arrow indicates reduction in signal amplitude for S_4^{2-} ions and the blue arrow, increase in S_3^- ions. **C** data from **B** with a constant offset of 0.05 for different visualization of peak changes overtime.

Conversely, reducing solution temperature discourages this behavior. Figure 10C offsets each UV-vis spectra by 0.05 a.u. of absorption to provide a different visualization of S_4^{2-} ions decreasing and S_3^- ions increasing during mild heating.

Based on the UV-vis study the discharge mechanism of sodium-sulfur was revisited at sub-ambient temperatures in the *in situ* optical cell. The G2 electrolyte was utilized since it delivered moderate behavior (between G1 and G4) at ambient. Over several replicates, it was observed that the discharge behavior, with identical electrode types and configuration, was different from at 20°C. Although the discharge was approximately the same duration, 0.98 h at 0°C, compared to 1.03 h at 20°C, cell voltage with respect to constant current was quite different. Both cells exhibit steady voltage first at 2.3 V but at 20°C this lasts for 0.6 h and at 0°C only 0.1 h. A second voltage regime is observed at ~1.9 V at durations of 0.8 and 0.2 h respectively. Finally, a third regime is observed at ~1.2 V at duration of 1.0 h at 20°C (close to termination) and 0.4 h at 0°C. At 20°C the first voltage regime (~2. 3V) dominates. We previously identified long chain polysulfide production in this region by viewing color change of the electrolyte (Figure 6-9). However, at 0°C the final voltage regime (~1.2 V) dominates. This portion of the discharge is expected to surpass the higher voltage regions,[6] and is where high-energy solid products are expected to deposit from the electrolyte back on the cathode leaving the electrolyte colorless (Figure 5). Since solvent viscosity decreases at low temperature, kinetics are slowed, hindering electrochemical performance. This likely explains the shortened high voltage regime at 0°C. However, the extended low voltage regime is advantageous to deliver the theoretical high energy of a sodium sulfur discharge.

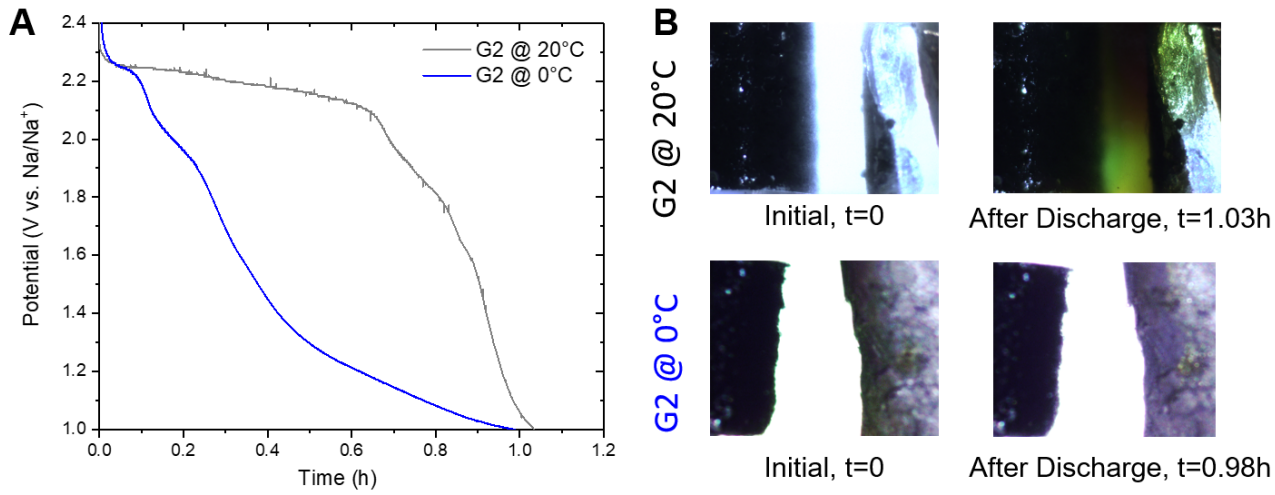

Figure 11- A Voltage during C/2 galvanostatic discharge in G2 at 20°C (grey) and 0°C (blue). **B** the electrolyte filled gap between the sulfur cathode (left) and sodium anode (right). Two cases are shown at each temperature: the initial case, and at the completion of a discharge in **A**.

Optical microscopy of the electrolyte gap during 0°C discharge revealed minimal color change (Figure 11), a surprising result in contrast to the dramatic color change observed at 20°C. This finding, as well as improved lower voltage or high-energy regime discharge, emphasizes the role of electrolyte viscosity in performance of this system and isolates operating temperature, as important design parameter for optimization. The finding is particularly intriguing when we consider that commercial sodium-sulfur systems operate at >300°C.[24] Future efforts will select

solvents for their system compatibility and modulate temperature for optimal viscosity to achieve high-energy discharge.

4. CONCLUSIONS

This work identifies optimal chemical (G1) and environmental environments (0°C) for the reaction between sodium and sulfur, so that this high energy pairing may be exploited for low cost energy storage ($1/kWh). It is of particular interest to naval applications that sub-ambient temperatures (here 0°C) enhance the system performance, since air and sea operations often require this temperature range. These findings were achieved using (1) UV-Vis characterization of polysulfide solubility, and (2) optical assessment of electrolyte color change combined with (3) electrochemical assessment of discharge duration.

One of the major successes of this work is providing a close to *operando in situ* environment for probing the ambient sodium-sulfur discharge reaction using optical microscopy. Despite the wide range of image brightness (20-80%) over the three *in situ* experiments, distinct sulfur speciation, diagnosed by RGB pixilation changes, can easily be correlated to features in the discharge voltage. This emphasizes the superiority of optical analysis over UV-Vis, which must maintain a much smaller brightness range (~20-50%), requiring very thin, impractical *in situ* cells. The wider concentration range, allows our measurements to approach *operando* conditions and will enable investigation of the full system, including the metallic sodium anode.

Using this technique we compare the *in situ* electrochemical discharge of sodium and sulfur in G1, G2, and G4, and find that the shorter the solvent chain length (G1), the higher the discharge capacity. The shortest chain glyme (G1) facilitates a longer discharge. The longer discharge delivers higher energy, since a more complete electrochemical reduction of sulfur occurs and chemical reordering in solution is minimized. This is identified by unexpected lower polysulfide solubility that we identified through UV-vis, and the suppressed polysulfide shuttling to the anode in G1 in the first discharge observed with optically.

Since the optimal glyme identified, G1, has a low flash point, a combination of glyme solvents or ethers may be required for a safe and high performance ambient sodium-sulfur battery electrolyte. Alternatively, when the ambient temperature is suppressed in a system with G2 electrolyte, the advantages observed in G1 are realized. Here a more complete reaction is observed and chemical reordering is suppressed. This finding provides an additional parameter to optimize electrolyte behaviors for ambient sodium-sulfur batteries. Further, sub-ambient environments are historically difficult for battery systems, so the advantaged operation of G2 in this condition is an exciting finding.

5. ACKNOWLEDGMENTS

Corey T. Love is acknowledged for supporting initial research, developing the first *in situ* optical cell, and sharing facilities. Vinh Nguyen, Optical Sciences Division, provided high quality, purified sulfur materials. Daniel Reed, Purdue Graduate student funded by NURP (Naval Undersea Research Program) performed optical and UV-vis experiments. Addison NewRingeisen processed images for RGB content, average color, and brightness.

6. ACCOMPLISHMENTS

Following this one year of effort, I was successful in pitching a 6.1 Base program optimizing electrode and electrolyte properties for ambient operation. The work was also presented at the 2019 MRS Fall Meeting and Exhibit in Boston, MA on December 1, 2019 and published in ACS Sustainable Chemistry and Engineering in early 2021.

REFERENCES

1. Tang, S.; Zhao, H., Glymes as Versatile Solvents for Chemical Reactions and Processes: from the Laboratory to Industry. *RSC Adv.* **2014,** *4* (22), 11251-11287.
2. Larcher, D.; Tarascon, J., Towards Greener and more Sustainable Batteries for Electrical Energy Storage. . Nature Chem, 2015; Vol. 7, pp 19-29.
3. Li, Z.; Pan, M. S.; Su, L.; Tsai, P.-C.; Badel, A. F.; Valle, J. M.; Eiler, S. L.; Xiang, K.; Brushett, F. R.; Chiang, Y.-M., Air-Breathing Aqueous Sulfur Flow Battery for Ultralow-Cost Long-Duration Electrical Storage. *Joule* **2017,** *1* (2), 306-327.
4. Manthiram, A.; Yu, X., Ambient Temperature Sodium–Sulfur Batteries. *Small* **2015,** *11* (18), 2108-2114.
5. Kumar, D.; Kuhar, S. B.; Kanchan, D. K., Room Temperature Sodium-Sulfur Batteries as Emerging Energy Source. *J. Energy Storage* **2018,** *18*, 133-148.
6. Wang, Y.-X.; Zhang, B.; Lai, W.; Xu, Y.; Chou, S.-L.; Liu, H.-K.; Dou, S.-X., Room-Temperature Sodium-Sulfur Batteries: A Comprehensive Review on Research Progress and Cell Chemistry. *Adv. Energy Mater.* **2017,** *7* (24), 1602829.
7. Wang, Y.-X.; Lai, W.-H.; Chou, S.-L.; Liu, H.-K.; Dou, S.-X., Remedies for Polysulfide Dissolution in Room-Temperature Sodium–Sulfur Batteries. *Adv. Mater.* **2020,** *32* (18), 1903952.
8. Pampel, J.; Dörfler, S.; Althues, H.; Kaskel, S., Designing Room Temperature Sodium Sulfur Batteries with Long Cycle-Life at Pouch Cell Level. *Energy Storage Mater.* **2019,** *21*, 41-49.
9. Li, T.; Xu, J.; Wang, C.; Wu, W.; Su, D.; Wang, G., The Latest Advances in the Critical Factors (Positive Electrode, Electrolytes, Separators) for Sodium-Sulfur Battery. *J. Alloys and Compd.* **2019,** *792*, 797-817.
10. Adelhelm, P. H., P.; Bender, C. L.; Busche, M.; Eufinger, C.; Janek, J., From Lithium to Sodium: Cell Chemistry of Room Temperature Sodium–Air and Sodium–Sulfur Batteries. *Beilstein J. Nanotechnol.* **2015,** *6*, 1016–1055.
11. Ohi, J. M. *Environmental, Health, and Safety Issues of Sodium-Sulfur Batteries for Electric and Hybrid Vehicles*; National Renewable Energy Lab., Golden, CO (United States): 1992.
12. Bao, C.; Wang, B.; Liu, P.; Wu, H.; Zhou, Y.; Wang, D.; Liu, H.; Dou, S., Solid Electrolyte Interphases on Sodium Metal Anodes. *Adv. Funct. Mater.* **2020**, 2004891.
13. Carter, R.; NewRingeisen, A.; Reed, D.; Atkinson, R. W.; Mukherjee, P. P.; Love, C. T., Optical Microscopy Reveals the Ambient Sodium–Sulfur Discharge Mechanism. *ACS Sustainable Chemistry & Engineering* **2021,** *9* (1), 92-100.
14. Love, C. T.; Baturina, O. A.; Swider-Lyons, K. E., Observation of Lithium Dendrites at Ambient Temperature and Below. *ECS Electrochem. Lett.* **2015,** *4* (2), A24-A27.
15. Atkinson, R. W.; Kingston, T. A.; Klein, E. J.; NewRingeisen, A.; Carter, R.; Love, C. T., Minimizing Lithium Deactivation during High-Rate Electroplating via Sub-Ambient Thermal Gradient Control. *Mater. Today Energy* **2020,** *18*, 100538.
16. Carter, R.; Parker, J. F.; Sassin, M. B.; Klein, E. J.; Wolak, M. A.; Love, C. T.; Long, J. W., Initiated Chemical Vapor Deposition of Ultrathin Polymer Coatings at Graphite Electrodes for Enhanced Performance in Li-Ion Batteries. *J. Electrochem. Soc.* **2020,** *167* (6), 060510.

17. Ryu, H.; Kim, T.; Kim, K.; Ahn, J.-H.; Nam, T.; Wang, G.; Ahn, H.-J., Discharge Reaction Mechanism of Room-Temperature Sodium–Sulfur Battery with Tetra Ethylene Glycol Dimethyl Ether Liquid Electrolyte. *J. Power Sources* **2011,** *196* (11), 5186-5190.
18. He, Q.; Freiberg, A. T. S.; Patel, M. U. M.; Qian, S.; Gasteiger, H. A., Operando Identification of Liquid Intermediates in Lithium–Sulfur Batteries via Transmission UV–vis Spectroscopy. *J. Electrochem. Soc.* **2020,** *167* (8), 080508.
19. Zou, Q.; Lu, Y.-C., Solvent-Dictated Lithium Sulfur Redox Reactions: An Operando UV–vis Spectroscopic Study. *J. Phys. Chem. Lett.* **2016,** *7* (8), 1518-1525.
20. Lowe, M. A.; Gao, J.; Abruña, H. D., Mechanistic Insights into Operational Lithium–Sulfur Batteries by in-situ X-ray Diffraction and Absorption Spectroscopy. *RSC Adv.* **2014,** *4* (35), 18347-18353.
21. Wenzel, S.; Metelmann, H.; Raiß, C.; Dürr, A. K.; Janek, J.; Adelhelm, P., Thermodynamics and Cell Chemistry of Room Temperature Sodium/Sulfur Cells with Liquid and Liquid/Solid Electrolyte. *J. Power Sources* **2013,** *243*, 758-765.
22. Morachevskii, A. G.; Demidov, A. I., Sodium–Sulfur System: Phase Diagram, Thermodynamic Properties, Electrochemical Studies, and Use in Chemical Current Sources in the Molten and Solid States. *Russ. J. of Appl. Chem.* **2017,** *90* (5), 661-675.
23. Zhang H, D. T., Qin B, Li H, Behm RJ, Passerini S., Solvent-Dictated Sodium Sulfur Redox Reactions: Investigation of Carbonate and Ether Electrolytes. *Energies* **2020,** *13* (4), 836.
24. Kumar, D.; Rajouria, S. K.; Kuhar, S. B.; Kanchan, D. K., Progress and Prospects of Sodium-Sulfur batteries: A Review. *Solid State Ion.* **2017,** *312*, 8-16.